Shahrekord University

Journal of Microfluidic and Nanofluidic Research

Journal homepage: https://jmnr.sku.ac.ir

Research Article

Analysis of Turbulence Intensity in a Gas-Solid Cyclone Separator

Sima Aghabali[1,2], Farshid Ghorbani Shahna[1,2*]

[1]*Occupational Health and Safety Research Center, Institute of Health Sciences and Technologies, Avicenna Health Research Institute, Hamadan University of Medical Sciences, Hamadan, Iran*

[2] *Center of Excellence for Occupational Health Engineering, School of Public Health, Hamadan University of Medical Sciences, Hamadan, Iran*

ARTICLE INFO

Article history:

Received: 2025-04-02

Revised: 2025-05-11

Accepted: 2025-05-16

Keywords:

Numerical simulation;
Turbulence intensity;
Gas-solid cyclone;
Collection efficiency;
Helical guide vane.

ABSTRACT

Turbulence intensity plays a critical role in determining the particle separation efficiency within gas-solid cyclones. While moderate turbulence enhances particle mixing and promotes effective collection, excessive turbulence can induce particle re-entrainment, thereby diminishing system performance. Parameters such as inlet velocity, particle size, and cyclone geometry are key contributors to the intensity of turbulence. Computational Fluid Dynamics (CFD) is extensively employed for optimizing cyclone design. This study investigates the variations in turbulence intensity across different cyclone configurations equipped with spiral guide fins. The findings reveal that cyclones incorporating 3.5 mm and 4.2 mm fins exhibit elevated turbulence levels, which are associated with increased energy dissipation and pressure drop. The maximum turbulence intensity is identified in the cyclone featuring a 2.8 mm fin and a pitch length of 1.25D. Interestingly, the presence of spiral fins leads to increased turbulence only under specific conditions, likely due to the greater number of fin turns, which amplify flow velocity and induce higher levels of disturbance.

1. Introduction

Gas-solid cyclones are indispensable devices in a wide range of industrial applications, serving as effective tools for the removal of particulate matter from gaseous streams. These separators are widely utilized in industries such as mineral processing, cement production, petroleum refining, biomass combustion, and air pollution control systems, where they contribute to emission reduction and process efficiency improvements [1, 2]. The fundamental operating principle of a cyclone relies on inertial separation, in which particles are subjected to centrifugal forces generated by a swirling gas flow. As the gas enters tangentially, it induces a vortex motion that forces denser solid particles toward the wall and ultimately down to the collection zone, while the cleaned gas exits through the central outlet [3, 4]. Continuous advancements in cyclone design have aimed at improving collection efficiency, especially for fine particles, while minimizing pressure drop to conserve energy. Key geometrical factors—such as cyclone diameter, body height, cone angle, vortex finder length, and inlet dimensions—have been systematically studied for their influence on performance [5, 6]. In particular, the adoption of spiral or helical guide vanes has gained attention for their ability to modify internal flow structures and enhance centrifugal forces, potentially improving separation [7, 8].

CFD has emerged as a vital tool in analyzing cyclone performance, enabling detailed insight into complex turbulent flow fields, particle trajectories, and pressure distributions [9, 10]. CFD facilitates the virtual testing of design configurations and operating conditions, offering

*** Corresponding author.**
E-mail address: *fghorbani@umsha.ac.ir*

Cite this article as:
Aghabali, S. and Ghorbani Shahna, F., 2025. Analysis of Turbulence Intensity in a Gas-Solid Cyclone Separator. *Journal of Microfluidic and Nanofluidic Research*, 2(2), pp. 91-99. https://doi.org/10.22034/jmnr.2025.15407.1014

both cost-effective and time-efficient pathways for optimization before fabrication and field implementation. Among various turbulence models, the Reynolds-Averaged Navier-Stokes (RANS) equations, along with k-ε and k-ω models, have been extensively employed in cyclone studies [11, 12].

The separation of fine particles remains a major challenge, particularly due to their tendency to follow the gas flow streamlines. Particle size distribution, density, and inlet velocity are among the most influential parameters governing collection efficiency [13, 14]. Addressing this issue requires a deep understanding of gas-solid flow behavior, particle-gas interactions, and turbulence intensity within the cyclone. Increasing turbulence generally enhances particle dispersion and residence time, aiding separation. However, excessive turbulence may promote particle re-entrainment, thereby reducing efficiency [15].

From an environmental and regulatory standpoint, efficient particulate removal is essential for controlling air emissions and maintaining compliance with air quality standards. This has become increasingly important as global regulations tighten around industrial emissions and sustainable practices [16]. Cyclones offer a low-maintenance, high-throughput option for pre-cleaning gas streams prior to finer filtration technologies, further highlighting their importance in industrial pollution control frameworks [17].

Despite technological progress, persistent issues such as material erosion, fluctuating gas composition, and non-uniform loading conditions continue to limit the consistent performance of cyclones across applications. Consequently, the development of hybrid systems, such as those combining cyclone separation with electrostatic precipitators or fabric filters, has been proposed to enhance efficiency and adaptability under variable operational conditions [18, 19].

This study aims to investigate the variations in turbulence intensity across gas-solid cyclone models incorporating helical guide vanes, with a focus on understanding how fin geometry affects internal flow characteristics and energy losses. Fig. 1 provides a schematic representation of the cyclone configurations evaluated in this study. Unlike previous works, this research provides a comparative analysis of turbulence intensity across multiple spiral fin dimensions and pitch lengths using CFD simulations, revealing specific configurations where turbulence is unexpectedly amplified. This nuanced insight contributes to the design of more energy-efficient and application-specific cyclone systems.

2. Governing Equations

Gas-solid separation in cyclones is governed by physical principles formulated through mathematical models that describe the behavior of both fluid and particulate phases. These equations provide a framework for predicting flow dynamics and optimizing cyclone performance across various industrial applications [4].

The gas phase is treated as a continuous fluid and modeled using the fundamental conservation laws. The continuity equation, ensuring mass conservation, is given by [20]:

$$\frac{\partial}{\partial t}(\rho) + \nabla \cdot (\rho \vec{u}) = 0 \tag{1}$$

where ρ is the gas density, t represents time, and $\vec{u}$ is the gas velocity vector.

The Navier-Stokes equation captures momentum conservation for the gas phase:

$$\frac{\partial}{\partial t}(\rho \vec{u}) + \rho(\vec{u} \cdot \nabla)\vec{u} = -\nabla p + \nabla \tau + \vec{F} \tag{2}$$

Here, p is the static pressure, τ is the shear stress tensor, and $\vec{F}$ represents the external body forces per unit volume, including gravitational and rotational influences.

For the discrete solid particles suspended in the gas stream, motion is governed by a force balance equation:

$$\frac{d\vec{u}_p}{dt} = F_D(\vec{u} - \vec{u}_p) + \frac{\vec{g}(\rho_p - \rho)}{\rho_p} + \vec{F}_r \tag{3}$$

where $\vec{u}_p$ is the particle velocity and ρ_p is the particle density. The term $\vec{F}_r$ encompasses rotational and history-dependent forces, including centrifugal, Coriolis, thermophoretic, Magnus lift, and Basset history effects.

The drag force, F_D, resulting from the relative motion between the particle and fluid, is expressed as [20]:

$$F_D = \frac{18\mu}{\rho_p d_p^2} \frac{C_D Re_p}{24} \tag{4}$$

where μ is the gas dynamic viscosity, C_D is the drag coefficient, d_p is the particle diameter, and Re_p is the particle Reynolds number:

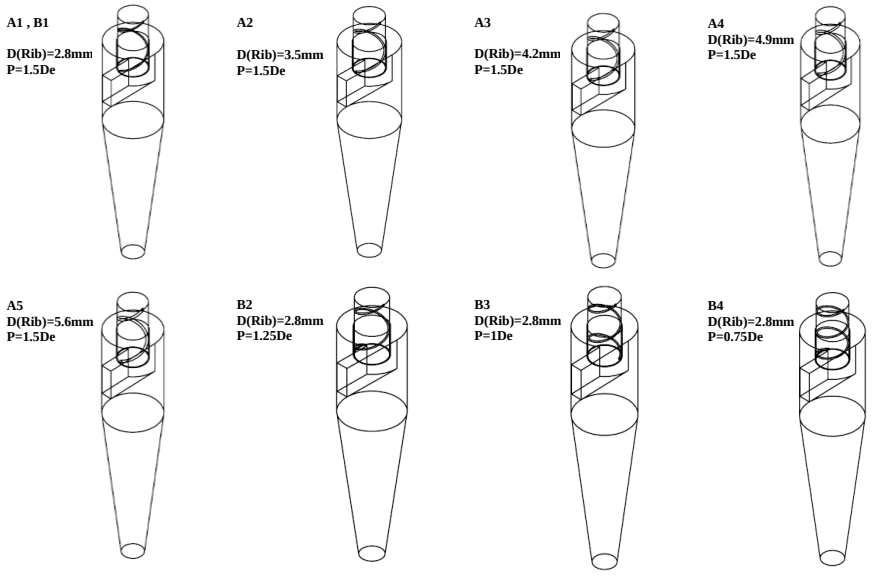

Fig. 1. Schematic of different cyclone models, where D_e indicates rib diameter and P is the pitch length.

$$\mathrm{Re_p} = \frac{\rho d_p \left|\vec{u} - \vec{u}_p\right|}{\mu} \tag{5}$$

The drag coefficient C_D for spherical particles can be estimated using [21]:

$$C_D = a_1 + \frac{a_2}{\mathrm{Re_p}} + \frac{a_3}{\mathrm{Re_p^2}} \tag{6}$$

where a_1, a_2, and a_3 are empirical constants derived for smooth spheres across a range of Reynolds numbers [22, 23]. For incompressible, turbulent flows of Newtonian fluids, the Reynolds-averaged Navier-Stokes (RANS) equations are used to model the mean momentum transport:

$$\frac{\partial \bar{u}_i}{\partial t} + \bar{u}_j \frac{\partial \bar{u}_i}{\partial x_j} = -\frac{1}{\rho}\frac{\partial \bar{P}}{\partial x_i} + \nu \frac{\partial^2 \bar{u}_i}{\partial x_i x_j} - \frac{\partial}{\partial x_j} \bar{u'}_i \bar{u'}_j \tag{7}$$

where $\bar{u}_i$ and $\bar{P}$ are the time-averaged velocity and pressure fields, respectively, and $\bar{u'}_i \bar{u'}_j$ denotes the Reynolds stress tensor. Since the RANS equations are unclosed, turbulence models are required to estimate this term. A more sophisticated closure approach is provided by the Reynolds Stress Model (RSM), which solves separate transport equations for each Reynolds stress component and includes dissipation effects. The general form of the RSM is [22]:

$$\begin{aligned} &\frac{\partial}{\partial t}(\bar{u'}_i \bar{u'}_j) + \bar{u}_k \frac{\partial}{\partial x_k}(\bar{u'}_i \bar{u'}_j) \\ &= \frac{\partial}{\partial x_k}\left(\frac{\nu_t}{\sigma_k}\frac{\partial}{\partial x_k}(\bar{u'}_i \bar{u'}_j)\right) \\ &- [\bar{u'}_i \bar{u'}_j \frac{\partial \bar{u}_j}{\partial x_k} \\ &+ \bar{u'}_i \bar{u'}_j \frac{\partial \bar{u}_i}{\partial x_k}] \\ &- C_1 \frac{\varepsilon}{k}[\bar{u'}_i \bar{u'}_j - \frac{2}{3} k \delta_{ij}] \\ &- C_2[P_{ij} - \frac{2}{3} P \delta_{ij}] \\ &- \frac{2}{3}\varepsilon \delta_{ij} \end{aligned} \tag{8}$$

with the turbulence production term given by:

$$P_{ij} = -[\bar{u'}_i \bar{u'}_j \frac{\partial \bar{u}_j}{\partial x_k} + \bar{u'}_j \bar{u'}_k \frac{\partial \bar{u}_i}{\partial x_k}], P = \frac{1}{2} P_{ij} \tag{9}$$

3. Results

Turbulence intensity plays a pivotal role in determining the separation efficiency of gas-solid cyclones. As the gas enters and circulates within the cyclone, complex interactions between the carrier phase and entrained solid particles give rise to intricate flow structures. Moderate levels

of turbulence enhance particle dispersion and promote effective mixing, which in turn facilitates particle migration toward the walls and improves collection efficiency. Conversely, excessive turbulence can destabilize the separation process by inducing particle re-entrainment into the gas core, thereby diminishing overall performance. Thus, maintaining an optimal turbulence regime is essential for achieving efficient and stable operation. Key parameters such as inlet gas velocity, particle diameter, and cyclone geometric configuration_particularly the inclusion of helical guide vanes_ exert significant influence on turbulence development. CFD is widely employed to investigate these effects and model the resulting flow fields with high spatial and temporal resolution. A detailed understanding of turbulence dynamics is instrumental in guiding cyclone design modifications, enabling energy-efficient configurations and reduced pressure losses, thereby optimizing industrial gas-solid separation systems both functionally and economically.

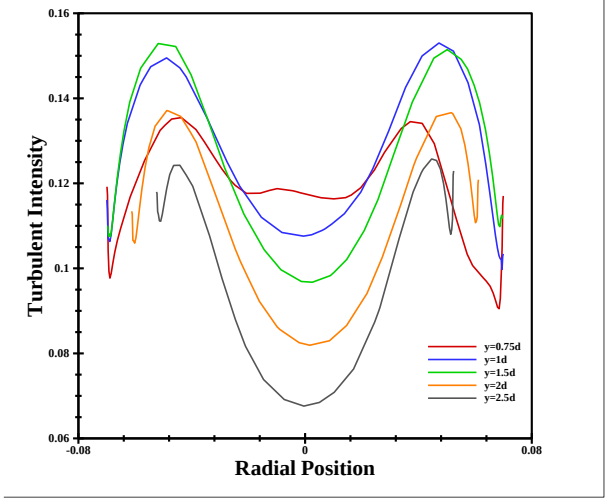

A1, B1

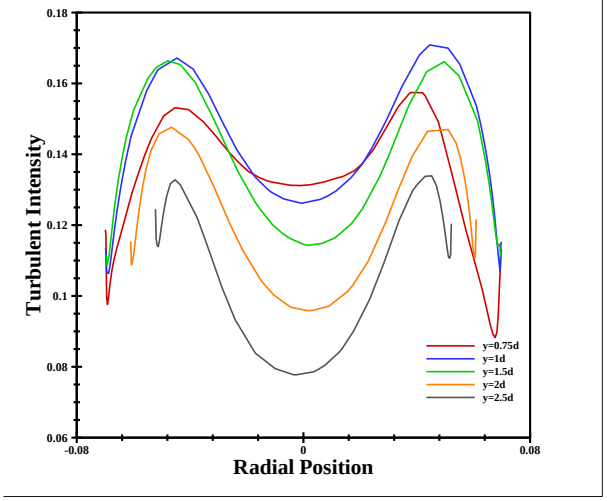

A2

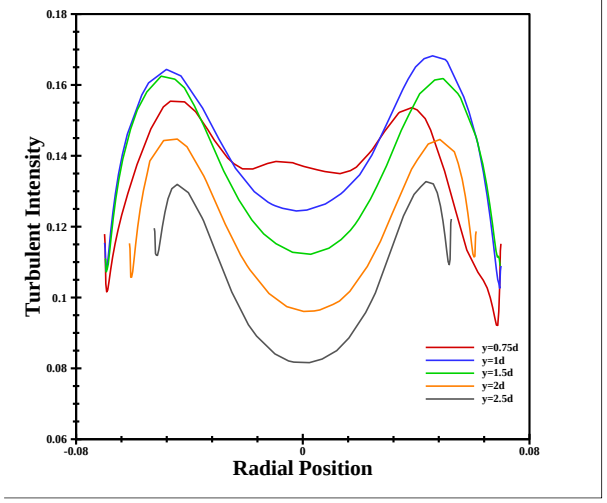

A3

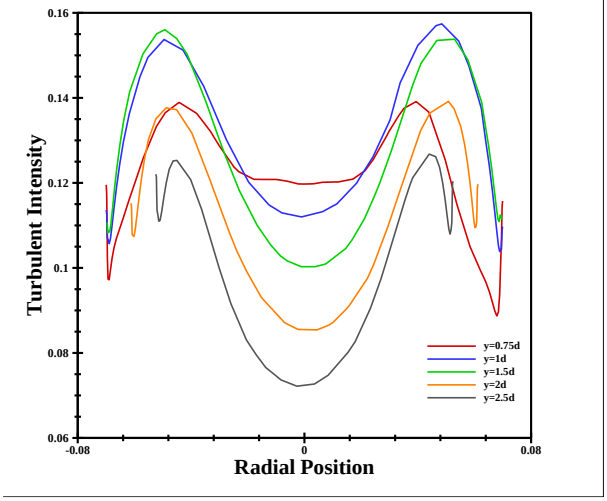

A4

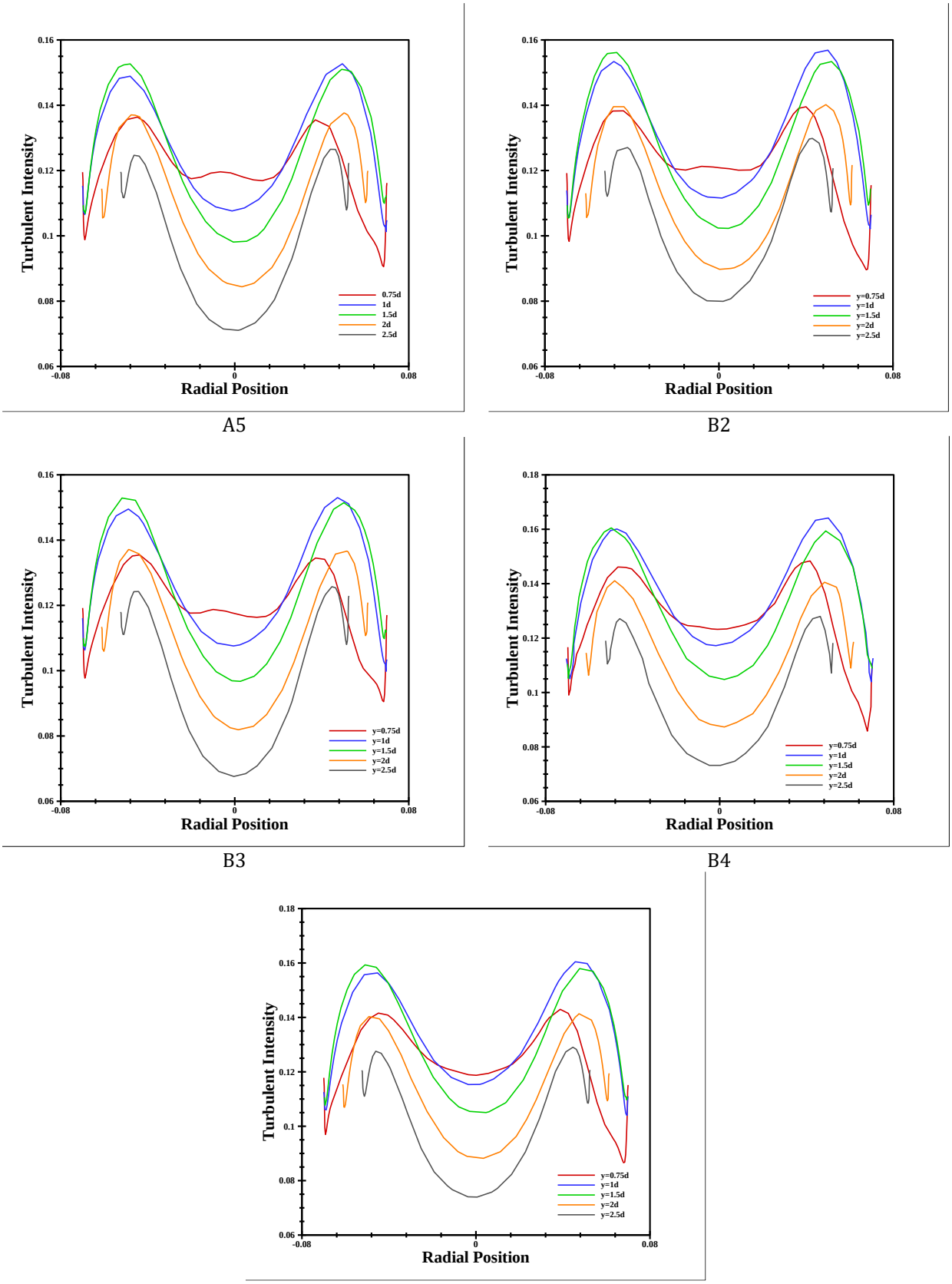

Fig. 2. The amounts of turbulence intensity for various cyclone models.

Fig. 2 sets A1–A5 and B1–B4, along with the reference cyclone, all exhibit the typical double-peaked turbulence intensity profile, with a maximum near the cyclone wall and a minimum at the centerline. This behavior reflects vortex-

driven flow characteristics and is consistent across axial positions (z=0.75D–2.5D).

Among the A-series, models A3 and A4 produce stronger turbulence near the wall, particularly at z=1.5D and 2.0D, indicating higher swirl and energy dissipation. A2 and A5, in contrast, show smoother gradients and lower peak intensities, suggesting more stable flow with reduced energy losses. A1–B1 lies in between, with turbulence levels stronger than A2 and A5 but less pronounced than A3.

In the B-series, B4 exhibits the highest turbulence intensity across the radial domain, followed by B2 and B3. These designs enhance swirl and particle separation potential, but at the cost of increased energy consumption.

The reference cyclone shows the lowest turbulence intensity overall, implying greater flow stability but weaker separation efficiency compared to modified geometries. Overall, the results highlight a trade-off: designs like A3 and B4 maximize swirl and turbulence, while A2, A5, and the traditional model prioritize flow stability and lower energy dissipation.

Fig. 3 highlights that, across all cyclone designs, the strongest turbulent zones are concentrated in the upper barrel region near the vortex finder and inlet. This localized peak originates from the sharp change in flow direction and high shear gradients where tangential velocity is introduced. The lower body and cone regions consistently display weaker turbulence, showing the natural decay of turbulent fluctuations as the swirling flow stabilizes and converges toward the dust outlet.

In the A-series, the behavior varies significantly with fin geometry. A1 and B1 generate moderate turbulence, with localized peaks confined near the vortex finder entrance. A2 and A4, on the other hand, show much higher turbulence, exceeding 40%, with red zones extending further into the cyclone body. These distributions indicate stronger swirl and shear, which intensify velocity gradients in the upper region. A3 maintains intermediate levels, around 36%, where the high-intensity zone is more compact compared to A2, suggesting a balance between strong turbulence and a contained distribution. A5 produces the lowest turbulence in the A-series, around 34.6%, with smoother gradients and smaller red regions, indicating a more stable and less dissipative flow field.

The B-series reveals another layer of contrast. B2 shows moderate turbulence, with localized intensities just under 39% near the vortex finder, pointing to a controlled flow pattern with limited spread of disturbances. B3 presents the highest turbulence intensity overall, close to 47%, with large red zones indicating extended regions of strong shear and velocity gradients. This makes it the most aggressive in terms of energy dissipation and swirl amplification. B4 also produces very high turbulence levels, around 44%, slightly below B3 but with a wider spread of high-intensity regions across the upper barrel. Both B3 and B4 clearly demonstrate how specific fin geometries amplify swirl far more than the moderate configurations.

Together, these contour plots provide a detailed spatial perspective of how turbulence develops and decays within different cyclone geometries. The distribution patterns underscore the role of fin size and pitch in controlling where turbulence is concentrated, how far it spreads from the vortex finder, and how strongly velocity gradients shape the flow inside the cyclone body.

Based on the turbulence intensity contours, all cyclone configurations show the strongest fluctuations near the inlet and vortex finder junction, where abrupt velocity changes generate pronounced shear layers. This localized peak consistently dominates the upper barrel region, while turbulence in the lower body and cone diminishes as the swirling flow converges toward the outlet, reflecting the natural decay of turbulent energy.

Among the A-series, distinct differences emerge according to fin geometry. Models A2 and A4 record the highest turbulence intensities, exceeding 40%, with elevated red zones that extend further into the upper barrel. These patterns indicate strong swirl amplification and enhanced shear forces, conditions that are associated with greater energy dissipation. In contrast, A3 maintains a more moderate maximum of around 36%, with its turbulent region confined to a smaller area, suggesting a balance between vigorous swirl and controlled energy loss. A1 and B1 show moderate peaks localized near the vortex finder, reflecting noticeable but less aggressive turbulence behavior, while A5 registers the lowest turbulence in the series (around 34.6%), characterized by smoother gradients and a more stable flow field.

The B-series demonstrates even stronger amplification in specific cases. B2 exhibits moderate turbulence, just under 39%, with intensity restricted to the vortex finder entrance, indicating a relatively controlled dissipation of energy. By contrast, B3 displays the highest turbulence intensity overall, approaching 47%, with a large high-intensity zone extending across the barrel, signifying significant shear and velocity gradients. B4 also shows very high turbulence levels (~44%), slightly lower than B3 but spread more broadly across the upper region of the cyclone. Together, B3 and B4 illustrate how

certain geometric configurations can drive nonlinear amplification of turbulence, far beyond the levels seen in other designs.

Taken collectively, these observations confirm that turbulence is not governed solely by fin size but also strongly influenced by pitch length and geometric arrangement. The spatial spread and intensity of turbulence vary considerably across designs, highlighting that fin-induced swirl can either be confined and controlled or amplified to levels that substantially alter flow dynamics. The contour distributions, therefore, underscore the sensitivity of cyclone performance to spiral fin geometry, as even small variations in diameter and pitch produce large differences in turbulence development and dissipation within the cyclone body.

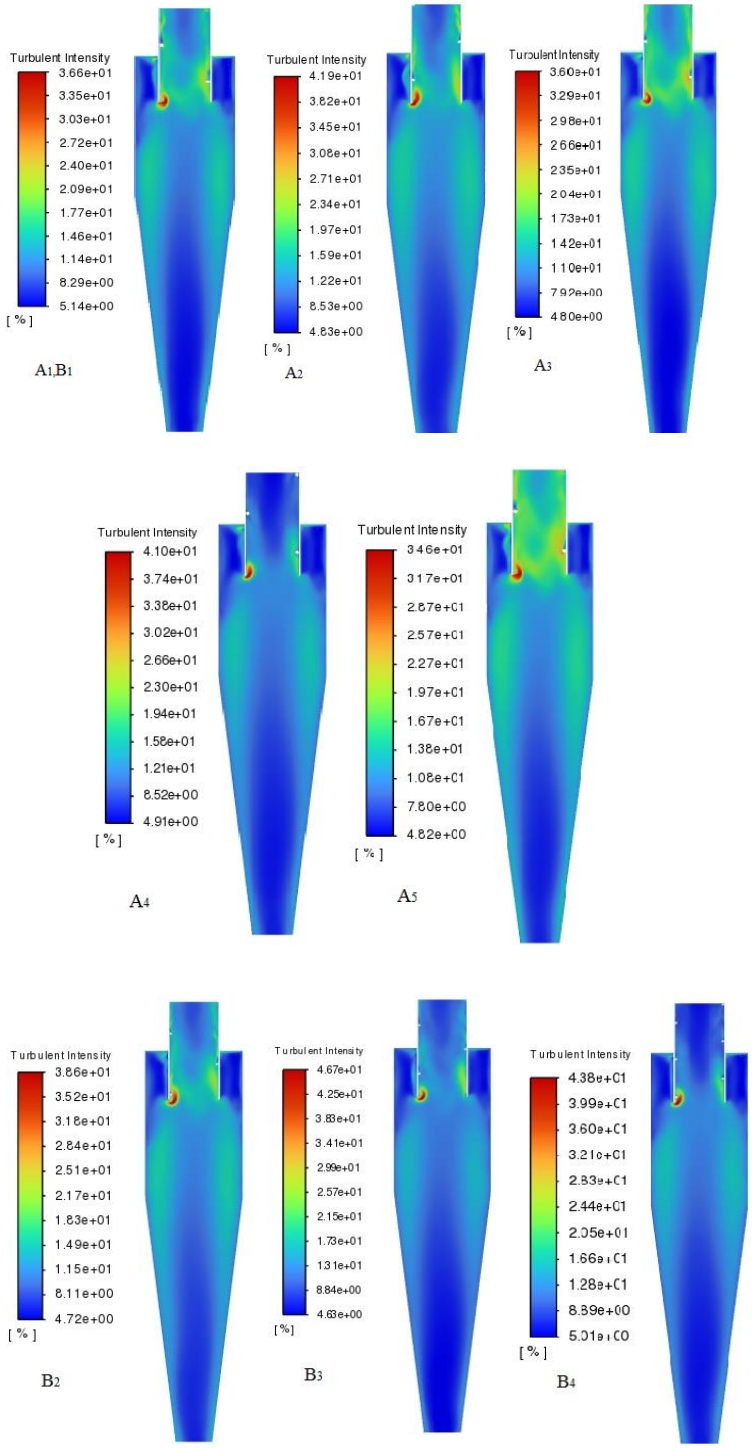

Fig. 3. Turbulence intensity contours for various cyclone models.

4. Conclusion

The analysis demonstrates that turbulence intensity in cyclones is highly sensitive to spiral fin geometry. Larger fin diameters (3.5 mm and 4.2 mm) and compact pitch lengths significantly amplify turbulence, leading to stronger swirl and higher energy dissipation, whereas smaller or longer-pitch fins (e.g., A5) generate smoother and more stable flow fields. Among all designs, models B3 and B4 show the highest turbulence intensities, highlighting the nonlinear effect of fin arrangement on flow dynamics. Conversely, the reference cyclone produces the lowest turbulence, offering greater stability but weaker separation forces. Overall, cyclone performance depends on balancing turbulence levels to ensure efficient particle separation without incurring excessive pressure drops or energy losses.

Reference

[1] Bayareh, M. (2024), A Review of the Experimental Analysis of Gas–Solid Cyclone Separators. ChemBioEng Reviews, 11, p. e202400036. https://doi.org/10.1002/cben.202400036

[2] Hsiao, T. C., Chen, D. R., and Son, S. Y., 2009. Development of mini-cyclones as the size-selective inlet of miniature particle detectors. Journal of Aerosol Science, 40(6), pp. 481–491. doi: 10.1016/J.JAEROSCI.2009.01.006

[3] Dehdarinejad E, Bayareh M, Ashrafizaadeh M (2021) A numerical study on combined baffles quick-separation device. Int. J. Chem. React. 19(5), pp. 515–526

[4] Dehdarinejad, E. and Bayareh, M., 2021. An Overview of Numerical Simulations on Gas-Solid Cyclone Separators with Tangential Inlet. ChemBioEng Reviews, 8(4), pp. 375–391. doi: 10.1002/cben.202000034

[5] Dehdarinejad E, Bayareh M (2021) Impact of non-uniform surface roughness on the erosion rate and performance of a cyclone separator, Chemical Engineering Science, 249, p. 117351, https://doi.org/10.1016/j.ces.2021.117351

[6] Ganegama Bogodage, S. and Leung, A. Y. T., 2016. Improvements of the cyclone separator performance by down-comer tubes. Journal of Hazardous Materials, 311, pp. 100–114. doi: 10.1016/J.JHAZMAT.2016.02.072

[7] El-Batsh, H. M., 2013. Improving cyclone performance by proper selection of the exit pipe. Applied Mathematical Modelling, 37(7), pp. 5286–5303. doi: 10.1016/J.APM.2012.10.044

[8] Dehdarinejad, E. and Bayareh, M., 2023. Analysis of the vortical flow in a cyclone using four vortex identification methods. Powder Technology, 428, pp. 118897. doi: 10.1016/J.POWTEC.2023.118897

[9] Raoufi, A., Shams, M., Farzaneh, M., and Ebrahimi, R., 2008. Numerical simulation and optimization of fluid flow in cyclone vortex finder. Chemical Engineering and Processing: Process Intensification, 47(1), pp. 128–137. doi: 10.1016/j.cep.2007.08.004

[10] Ganegama Bogodage, S. and Leung, A. Y. T., 2015. CFD simulation of cyclone separators to reduce air pollution. Powder Technology, 286, pp. 488–506. doi: 10.1016/J.POWTEC.2015.08.023

[11] Chauhan, J., Salvi, B. L., Khidiya, M. S., and Agrawal, C., 2022. Computational Fluid Dynamic Analysis of Cyclone Separator for Flue Gas Cleaning by Using Standard k-Epsilon Model. doi: 10.1007/978-981-16-8341-1_2

[12] Gronald, G. and Derksen, J. J., 2011. Simulating turbulent swirling flow in a gas cyclone: A comparison of various modeling approaches. Powder Technology, 205(1–3), pp. 160–171. doi: 10.1016/j.powtec.2010.09.007

[13] Vermande Paganel, T., Fabrice Alban, E., Cyrille, M. A., and Ngayihi Abbe, C. V., 2024. CFD Simulation of an Industrial Dust Cyclone Separator: A Comparison with Empirical Models: The Influence of the Inlet Velocity and the Particle Size on Performance Factors in Situation of High Concentration of Particles. Journal of Engineering, doi: 10.1155/2024/5590437

[14] Tang, Z., Yu, L., Wang, F., Li, N., Chang, L., and Cui, N., 2018. Effect of Particle Size and Shape on Separation in a Hydrocyclone. Water, 11(1), pp. 16. doi: 10.3390/w11010016

[15] Jafari, P. H., Hellström, J. G. I., and Gebart, B. R., 2017. Turbulence Modelling of a Single-Phase Flow Cyclone Gasifier. Engineering, 09(09), pp. 779–799. doi: 10.4236/eng.2017.99047

[16] Gutierrez, J. A., Guerrero Narvaez, J. A., Campo Ceballos, D. A., and Muñoz Chaves, J. A., 2024. Development of a cyclone separator for particulate matter control in fique bag production: A case study at Empaques del Cauca S.A. Case Studies in Chemical and Environmental Engineering, 10, p. 100951. doi: 10.1016/J.CSCEE.2024.100951

[17] Dziubak, T. and Bąkała, L., 2021. Computational and Experimental Analysis of Axial Flow Cyclone Used for Intake Air Filtration in Internal Combustion Engines. Energies, 14(8), p. 2285. doi: 10.3390/en14082285

[18] Dehdarinejad, E. and Bayareh, M., 2022. Impact of non-uniform surface roughness on the erosion rate and performance of a cyclone separator. Chemical Engineering Science, 249, p. 117351. doi: 10.1016/j.ces.2021.117351

[19] Castro, B. J. C. de, Sartim, R., Guerra, V. G., and Aguiar, M. L., 2020. Hybrid air filters: A review of the main equipment configurations and results. Process Safety and Environmental Protection, 144, pp. 193–207. doi: 10.1016/J.PSEP.2020.07.025

[20] Ci, H. and Sun, G., 2015. Effects of Wall Roughness on the Flow Field and Vortex Length of Cyclone. Procedia Engineering, 102, pp. 1316–1325. doi: 10.1016/J.PROENG.2015.01.262

[21] Dehdarinejad, E., Bayareh, M., 2023.Performance analysis of a novel cyclone separator using RBFNN and MOPSO algorithms. Powder Technology, 426, p. 118663, https://doi.org/10.1016/j.powtec.2023.118663

[22] Launder, B. E., Reece, G. J., and Rodi, W., 1975. Progress in the development of a Reynolds-stress turbulence closure. Journal of Fluid Mechanics, 68(3), pp. 537–566. doi: 10.1017/S0022112075001814